Jurnal Kejuruteraan 34(5) 2022: 965-973
https://doi.org/10.17576/jkukm-2022-34(5)-25

Anomaly Gait Detection in ASD Children based on Markerless-based Gait Features

Nur Khalidah Zakaria[a], Nooritawati Md Tahir[* a,b,c], Rozita Jailani[a] & Mayada M Taher[d]

[a]*College of Engineering, Universiti Teknologi MARA, Selangor, Malaysia.*
[b]*Institute of Big Data Analytics and Artificial Intelligence (IBDAAI), Universiti Teknologi MARA, Malaysia.*
[c]*Integrative Pharmacogenomics Institute (iPROMISE), Universiti Teknologi MARA, Selangor, Malaysia.*
[d]*Laser and Optoelectronics Engineering Department, University of Technology, Baghdad, Iraq.*

[*]*Corresponding author: nooritawati@ieee.org*

Received 09 January 2022, Received in revised form 13 March 2022
Accepted 12 April 2022, Available online 30 September 2022

ABSTRACT

Children with autism are known for their difficulties in social interaction, communication, and behaviour characteristics. Hence, this study proposed to develop a markerless-based gait method for anomaly gait detection in children with autism spectrum disorder (ASD). Firstly, a depth sensor is used during walking gait data collection of the 23 ASD children and 30 typical healthy developing (TD) children. Further, these walking gait data are divided into the Reference Joint (REF) and Direct Joint (DIR) features. For each type, five sets of features are derived that represents the whole body, upper body, lower body, the right and left side of the body. The three classifiers used to validate the effectiveness of the proposed method are Naïve Bayes (NB), Support Vector Machine (SVM), and Artificial Neural Network (ANN). Results showed that the highest accuracy, precisely 94.22%, is achieved using the ANN classifier with DIR1 gait features representing the whole body. The highest sensitivity and specificity obtained are 94.49% and 93.93% accordingly. In addition, the proposed markerless model using the DIR1 gait features and the ANN as classifier also outperformed previous studies that have utilised the marker-based model. This promising result showed that the proposed method could be used for early intervention for the ASD group. The markerless-based gait technique also has fewer experiment protocols, thus causing the ASD children to feel more comfortable.

Keywords: ASD children; autism; gait classification; gait features; markerless-based.

INTRODUCTION

Screening and diagnosis of ASD are based on the criteria categorised by several problems, including the communication, learning process, and social skill as listed in The Diagnostic and Statistical Manual of Mental Disorder, fifth edition (DSM-5) (S. J. Spence et al. 2004). Unfortunately, there is no specific indicator to detect the disorder related to the motor impairment and any altered gross movement function in children with ASD motor. To the extent of our knowledge, there is no cure for this type of deficit (E. I. de Bruin et al. 2015 & M. S. Nadeem et al. 2020). Numerous studies have discussed movement and sensory disturbances (C. Armitano et al. 2020 & H. L. Miller et al. 2019) unbalanced movement, especially during walking (J.D. Eggleston et al. 2018). This is because gait characteristics or features may potentially be used as an early indicator in detecting gait abnormality among ASD children (L. Gong et al. 2020, C. Z. C. Hasan et al. 2018 & J.D. Eggleston et al. 2020). Thus, gait analysis can be a promising method for analysing the gait behaviours in ASD children. Note that several techniques were developed for gait monitoring purposes. For example, inertia sensors were attached to ASD participants' feet, legs, arm, pelvis, and thoracic spine to capture the gait kinematics features and analyse the age groups' gait symmetry (Y. Li et al. 2021). In another study, a plantar pressure mat was placed in the middle of the carpet to measure the foot-ground interaction and gait characteristics (L. Gong et al. 2020). The marker-based approach includes an optoelectronic system with synchronisation between the electronic devices. Here the system produced the three-dimensional (3D) model from the trajectories of the markers (M. Leo et al. 2017) and the floor-sensor as the third-party equipment from the optoelectronic gait system as reported in (J.S. Dufek et al. 2017, S. Ilias et al. 2016, M. Calhoun et al. 2011).

Conversely, the markerless-based technique is markers free and usually involved algorithms development (M. Nieto-Hidalgo et al. 2016). Cocchi et al. (2017) used the depth sensor to estimate the sagittal joints kinematics of children with cerebral palsy, followed by validation of kinematic features versus marker-based measurements. Meanwhile, M. Nieto-Hidalgo et al. (2015) used dynamic parameters from the heel-strike and toe-off events based on algorithms developed using the side view of subjects' walking. Results attained showed a success rate of more than 90% accuracy. Further, spatiotemporal parameters such as stride time, step length, step time and double support time were derived

based on the body points output from the depth sensor in gait assessment of children with cerebral palsy as discussed by C. C. Barreira et al. (2020). Conversely, K Jun et al. (2020) reported method developed by dividing the skeletal data into different groups to identify the unimportant joints that contributed to low impact in classification for five types of pathological gait.

One of the main challenges in gait analysis research is during the data acquisition stage (K. Pope et al. 2020). Since most of the data acquisition process was performed in the laboratory environment, children with ASD might lose focus or confront anxiety due to the unfamiliar laboratory environment. ASD children must wear tight-fitting clothes, and sensors or reflective markers must be attached to their clothes or body during data acquisition and experiment (B.O. Lim et al. 2016). Despite the abnormal gait associated with ASD, many uncertainties exist concerning this complex neurological disorder (O. Manicolo et al. 2021). More studies need to be conducted in analysing the gait features of the ASD subjects by employing the gait features and computer vision intelligence techniques (K. Pope et al. 2020). It is hypothesised that a suitable gait method can be proposed as a possible gait monitoring technique to support the early diagnosis of ASD gait, which is more apt for ASD children known for their difficulties in behavioural characteristics.

Therefore, this study aims to propose and develop markerless-based gait features for anomaly gait detection in children with ASD. The potential gait features will be used to classify the gait of ASD versus TD group. Here, Artificial Neural Network (ANN), Naïve Bayes Classifier (NBC) and Support Vector Machine (SVM) are used to validate the accuracy of the gait features. In addition, this study aims to address challenges in gait analysis based on markerless-based gait techniques. New insights on ASD are proposed, possibly to help determine the degree of deficits specificity and the development of valuable tools that can be used to analyse the walking gait of ASD children.

METHODOLOGY

This section elaborates the overall methodology used in this work. As shown in Figure 1, the proposed method comprises four phases: data acquisition, pre-processing, gait features representation, and classification.

DATA COLLECTION

Data collection was based on 30 TD and 23 ASD subjects; between 5 to 12 years of age. The experimental setup for data acquisition purposes was held in the Human Motion and Gait Analysis (HMGA) UiTM Selangor. Based on the UiTM Research Ethics Committee (REC) approval, parents or guardians must complete the consent form and all the required information. A Kinect sensor, specifically a depth camera, is used to record the markerless-based gait data during the data acquisition stage. Table 1 tabulated the summary of demographic and anthropometric data for the two groups. In this study, 14 males and 16 females were recruited for the TD group. Note that this study is not focused on gender-based groups.

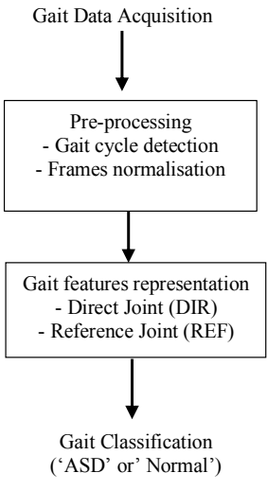

TABLE 1. Summary of Demographic and Anthropometric Data for Both ASD and TD Groups.

Items	Mean	(Standard Deviation)
	ASD Group	TD Group
Gender (F:M)	(2:21)	(16:14)
Age (year)	8.30 (0.396)	9.03 (0.419)
Weight (kg)	32.96 (3.485)	32.49 (1.991)
Height (m)	1.27 (0.0028)	1.32 (0.0025)
BMI (kg/m2)	19.51 (1.297)	18.22 (0.644)

On the other hand, both groups have eight months difference where the TD group has a mean value of 9.03 years old and the ASD group has a mean value of 8.39 years old. In addition, the difference in height for both groups is 4.9 cm, where the TD group is slightly taller than the ASD group, with a size mean of 1.32 m and 1.27 m, respectively. Meanwhile, the mean difference in weight is 0.47 kg with the ASD group is heavier and has higher weight; meanwhile, the BMI of the ASD group is higher with a difference of 1.29 kg/m² as compared to the TD group.

Next, the Kinect sensor and camera are set at 30 Hz and working range of between 1.2 to 3.5 meters along with the horizontal field view set at 57° wide. Further, the sensor provided a vertical field view of 43°. The tilt motor system can enhance the field view by allowing the sensor to be tilted up or down up to 27° in either direction. During data acquisition, the Kinect sensor is placed at the height of 0.5 meters from the floor and facing the walking path. For this device, the global coordinate system or the origin ($x=0, y=0, z=0$) is located at the centre of the IR sensor on Kinect, where x and y are the sensor's left and right in the sensor's

point-of-view and z is the sensor direction facing subject's while walking with 1 unit equals to 1 meter.

For the experimental and analysis, subjects are requested to perform their walking task via their normal and comfortable walking speed without using any walking aid or assistance. A minimum of ten walking sessions are acquired from the normal group of children. For the ASD group, the data acquisition process is done until the walking gait video sequences acquired were sufficient and apt for analysis and, of course, with the consent and as agreed by their guardian. Further, the skeleton viewing and skeleton tracking functions are used to track the subject as the subject performs the walking trial. These algorithms represent the depth coordinates that provide detailed information of the twenty body skeleton points by the depth values measured between the camera and body. Figure 2 illustrates an example of an output image from the camera. Here, Figure 2(a) is the RGB output, Figure 2(b) is the depth sensor output, and Figure 2(c) is the skeleton viewing function output that provides the skeleton model consisting of the twenty (20) body points.

DATA ANALYSIS

Gait cycle detection is carried out to extract the gait features within the entire gait cycle. One complete gait cycle is described as the interval between two successive events during walking. For example, once the subject started walking via landing his right foot and completing his gait cycle, he would perform the same foot's next landing. Next, the extracted gait cycle is normalised for each trial for the exact size of the frame number. Based on equation (1), the distance between ankles, $d\ (a,\ b)$ is calculated to determine the gait cycle where a is the left ankle joint whilst b is the right ankle joint in x, y, and z axes, respectively. The gait cycle is detected by calculating the three consecutive local maxima (R. Sahak et al. 2017).

$$d(a,b) = \sqrt{(x_a - x_b)^2 + (y_a - y_b)^2 + (z_a - z_b)^2} \quad (1)$$

Further, Figure 3(a) illustrates an example of gait cycle detection. Figure 3(a) shows that there are one to three gait cycles in one successful trial. Only one gait cycle was selected for each walking trial per subject as depicted by the two vertical dashed lines to avoid biased performance in the subsequent analysis stage. Figure 3(a) also illustrates the calculated distance between ankles, and the three consecutive local maxima are detected at frames 2 to 6, as marked by the two vertical dashed lines. The left and right ankles projection points in the z-axis (C. C. Barreira et al. 2020) are plotted and labelled as Figure 3(a), determining the heel strike and toe-off events. The local maxima represent the maximum distance peak between the ankle's points. Thus, the first local maximum is the first occurrence of heel-strike during the initial contact event. The foot-off during the terminal stance event represents the second maximum peak. The third local maximum peak is the second occurrence of heel strike during the terminal swing event of the same foot.

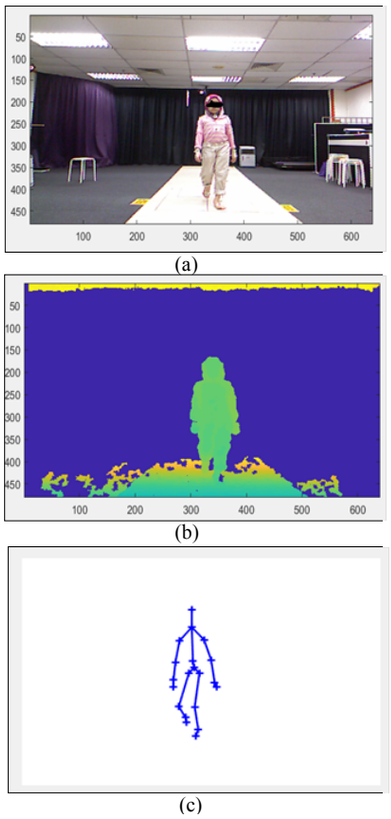

FIGU ːct Depth Sensor: (a) RGB image output, (b) depth image output, and (c) twenty body points skeleton model output.

Next, the extracted gait cycle consists of different frames due to various walking speeds even though these frames are removed from the same subjects. Thus, the interpolation technique is applied to standardise and fix at the 30th frame for each trial (F. Sun et al. 2020). Figure 3(b) illustrates the output of frame normalisation. Here, the spline interpolation technique is used since spline interpolation is suitable to approximate new values within the skeletal data points (R. Sahak et al. 2017). As depicted in Figure 3(b), the number of frames before synchronisation is five, and the skeletal data in each frame are plotted as shown by the horizontal lines. Next, the number of frames for each walking trial is set at 30 frames. After the frames are normalised, the skeletal data are plotted again. From Figure 3(b), the plotted skeletal data showed similar patterns and values upon synchronisation completion.

FEATURE REPRESENTATION

As mentioned earlier, the proposed markerless-based gait features used in this study for anomaly gait detection of the ASD gait is based on the twenty skeleton joints in the three

dimensional (3D) form as shown in Figure 4 that generated a total of 60 skeleton joint points. The data of skeleton data can be divided into two types: Reference Joint features (REF) and Direct Joint (DIR).

Refer to Table 2, for each type; five feature sets are derived to represent the whole body, upper body, lower body, the right side, and the left side of the subject's body, specifically DIR1, DIR2, DIR3, DIR4 and DIR5 followed by REF1, REF2, REF3, REF4 and REF5. These features are further used to evaluate and verify in-depth the ability of each feature amongst these five sets that could discriminate the walking gait of these two groups, namely ASD and TD children.

Dir Gait Features

The DIR features are represented by the selected body point and the respective depth information as tabulated in Table 2. Figure 4(a) shows that DIR Set 1 consists of 20 body points representing one set for the entire body. The detail of each DIR feature is described in Table 2.

Ref Gait Features

Referring to Figure 4(b), REF Set 7 consists of features for the upper body points.

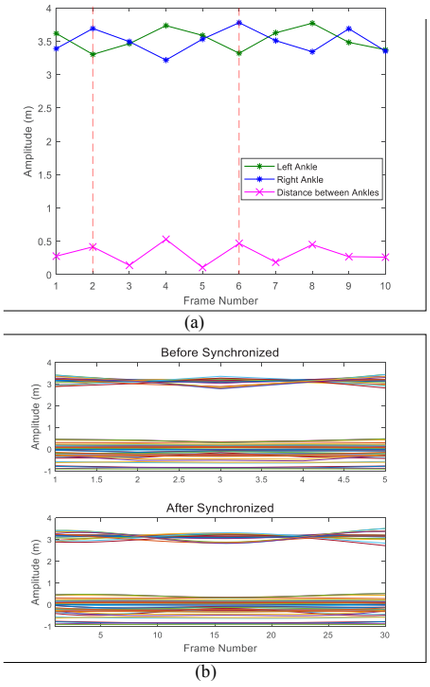

FIGUI tion
as ill cycle detection as illustrated by two vertical me
normalisation

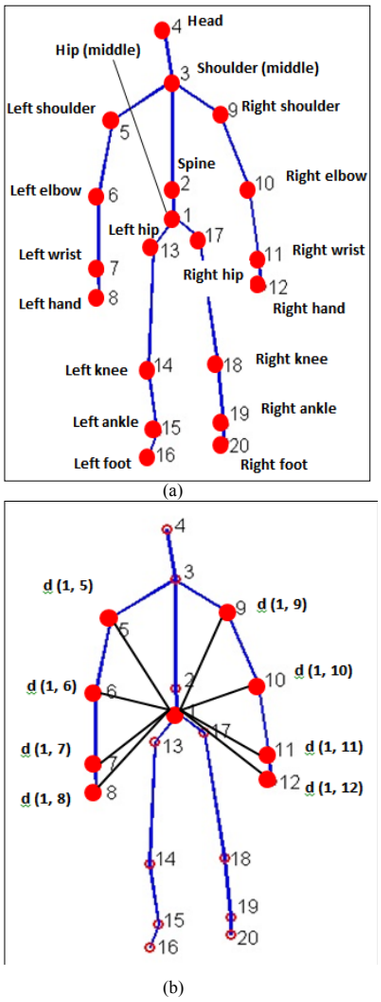

FIGURE 4. Example of illustrations for (a) selected body point for DIR Set 1 and (b) selected distance for REF Set 7.

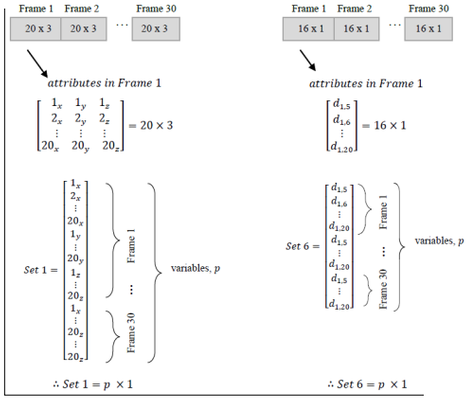

ion

TABLE 2. Description for DIR and REF Type

Feature	Description (Body Point)
DIR1	Set for the full-body by choosing the entire body points in the x, y, and z axes (1 to 20)
DIR2	Set for the upper body and extracted by selecting the body points on the upper body in the x, y, and *z* axes (2 to 12)
DIR3	Set for the lower body and extracted by selecting the body points on the lower body in the x, y, and z axes (1, 2, and 13 to 20)
DIR4	Set for the right sides of the body and extracted by selecting the body points on the right side in the x, y, and z axes (1 to 4, 9 to 12 and 17 to 20)
DIR5	Set for the left side of the body and extracted by selecting the body point on the left side in the x, y, and z axes (1 to 8 and 13 to 16)
REF6	Set for the full-body and extracted by calculating the distance between the reference joint to all body joints (Reference point to point 5 to 20)
REF7	Set for the upper body and extracted by calculating the distance between the reference joint to the joint's points on the upper body (Reference point to point 5 to 12)
REF8	Set for the lower body and extracted by calculating the distance between the reference joint to the joint's points on the lower body (Reference point to point 13 to 20)
REF9	Set for the right sides of the body and extracted by calculating the distance between the reference joint to the joint's points on the right side (Reference point to point 9 to 12 and 17 to 20)
REF10	Set for the left side of the body and extracted by calculating the distance between the reference joint to the joint's points on the left side (Reference point to point 5 to 8 and 13 to 16)

The REF features are represented by the distance feature based on the distance between the reference joint located at the middle hip (Point 1) and the other selected body joint computed using Euclidean distance as in equation (1). The detailed description of each REF feature is as in Table 2.

Next, frames of each set feature are arranged vertically concatenated. The purpose of the concatenation is to adapt the input properties for the classification stage. The output of each trial has a dimension of $p \times 1$, where p is the total attributes or variables in each sample or walking trial. The examples of the attributes concatenation for Set 1 and Set 6 are as illustrated in Figure 5. Table 3 tabulates the description of the total body points.

TABLE 3. Description of number of body points and number of variables for DIR and REF features

Feature	Total body points per frame	*p* (Vertical concatenated)
DIR1	20 x 3	1800
DIR2	11 x 3	990
DIR3	10 x 3	900
DIR4	12 x 3	1080
DIR5	12 x 3	1080
REF6	16 x 1	480
REF7	8 x 1	240
REF8	8 x 1	240
REF9	8 x 1	240
REF10	8 x 1	240

Note that for Set 1 to Set 5, the selected body points are multiplied by three as in Figure 5 because these sets consist of depth information specifically in the *x, y*, and *z* axes. On the other hand, for Set 6 to Set 10, the selected distances are multiplied by one because the distance is calculated based on the *x, y*, and *z* axes between the two body joints. These features are arranged vertically concatenated for each trial via frame by frame. Hence, each set of features has a dimension of p by 300 after combining the trials concerning its group.

Gait Classification

Upon identifying the gait feature, the next stage is to assess the efficacy of the markerless-based gait features for anomaly gait detection in ASD children based on the two categories, namely DIR and REF sets. Each dataset is classified and evaluated using three types of classifiers: the Artificial Neural Network (ANN), Support Vector Machine (SVM), Naïve Bayes Classifier (NBC). The classifier's output is set as either ASD or TD groups. The target for the ASD group is '0', and the TD Group is '1'. A 10-fold cross-validation method is applied to estimate the generalization error of each classifier.

Support Vector Machine (SVM) As Classifier

SVM is a linear classifier that aims to classify features by determining the finest hyperplane. The best hyperplane for SVM is the most significant margin separating the features between different classes (N. M. Tahir et al. 2007). This is obtained by balancing the margin maximization using regularization parameter C. However, not all data are linearly separable in the actual application and can be separated using the hyperplane. Thus, for non-linear problems, soft margins and kernel functions have been introduced. The

kernel's role is to transform the input data into the required form in suitable feature space for separating the hyperplane. Here, the linear, radial basis function along with the polynomial kernels are utilised as the kernel functions. The kernel functions are used to compute the xj and xk in V (xj, xk) where j and k are the observations in predictor data, x as tabulated in Table 4.

TABLE 4. Kernel function of SVM

Kernel Function	Mathematical Formula
Linear	$V(x_j,x_k) = x_j' x_k$
RBF	$V(x_j,x_k) = \exp(-\gamma \| x_j - x_k \|^2)$ where γ is the width of RBF kernel
Polynomial	$V(x_j,x_k) = (1 + x_j' x_k)^{dp}$ where *dp* is the degree of polynomial

Naïve Bayes (NB) As Classifier

NB classifier is a supervised algorithm based on Bayesian learning algorithm derived from decisions of probabilistic classification. The algorithm uses the Bayes theorem and naively presumes the entire predictors are independent considering each class value. This conditional independence assumption is seldom applicable in real or practical applications, and because of this, it is characterised as Naive. Conversely, in various controlled classification problems, the algorithm tends to learn rapidly. According to Bayesian Theorem, the probability of a data predictor is as in equation (2):

$$P(c|x) = \frac{P(x|c) * P(c)}{P(x)} \quad (2)$$

Using the theory, the probability of x is happening, given that *c* has occurred, where $P(c|x)$ is the posterior probability of class (c, target) given the data or predictor (*x*, attributes). Conversely, P(c) is the prior probability of a class, $P(x|c)$ is the probability of predictor given by the class, and $P(x)$ is the probability of the predictor. The assumption made here is that the predictors or features *x* are independent; that is, the presence of one particular feature does not affect the other. Hence it is called naïve (H. Bakhta et al. 2009). For classification purposes, the probability distribution function is used to model the data using kernel density estimation or Gaussian distribution. The two categories of probability distribution functions are kernel density estimation along with Gaussian distribution. The mean and standard deviation of each class's training data is computed, and the NBC estimates a separate normal distribution for each.

Artificial Neural Network (ANN) As Classifier

ANN emulates the human brain's learning process that can solve problems involving complex and nonlinear data. The ANN architecture comprises the input, hidden, and output layers. ANN performs its processing by accepting input, *x*, multiplied by a set of weights, *w*. Then, the neurons will non-linearly transform the sum of the weighted inputs using an activation function into an output value, *y*, as shown in equation (3) (S. Ilias et al. 2016). Sometimes *b*, a bias regarded as weight is also added to the network. The network will continuously adjust the parameters to achieve the tolerable desired output.

$$y = \sum_{i=1}^{n} w_i x_i + b \quad (3)$$

For this study, ANN with three-layer feed-forward architecture with Scaled Gradient Conjugate as the training algorithm and tan-sigmoid (tansig) transfer function is utilised for both the hidden and output layer.

Tune Hyperparameters For Classification

In this study, hyperparameters are evaluated and tested to fit the algorithm's performance to the dataset. The evaluations from each classifier model are performed using a grid search approach to select the optimal classifier model. The hyperparameters for each classifier are as tabulated in Table 5.

TABLE 5. Hyper-parameters

Classifier	Hyper-parameter	Variable/Value
SVM	Kernel	*C* (*C* ϵ 0.001, 0.01, 0.1, 1, 10, 100 and 1000) for linear kernel;
		C and γ (γ ϵ 0.1, 1 and 10) for RBF kernel;
		C and *dp* (*dp* ϵ 2, 3 and 4) for polynomial kernel
NB	Probability distribution	Kernel density distribution.
		Normal distribution.
ANN	Hidden neurons	*hn* (*hn* varied from 1 to 50 with an increment of 5)

RESULTS AND DISCUSSION

This section discusses the classification and performance of each set of features based on each classifier. For performance measure, the accuracy (Acc) is defined as a reflection of actual value or the ability of a measurement to be correct. On the other hand, sensitivity (Sens) is defined by the correct classification of the ASD in the ASD group, whilst specificity (Spec) is determined by the correct classification of the TD in the TD group. Table 6 tabulated the classifier performances for DIR and REF feature sets. Firstly, with SVM as classifier using all three kernels as tabulated in Table 4, experimental results showed that the highest accuracy for linear kernel is only at 86.83%

accuracy using DIR Set 1, while for the polynomial kernel, the highest accuracy is at 88% using DIR Set 2. RBF Kernel showed the highest accuracy amongst these three kernels for DIR and REF feature sets with generalization parameter C=10. Hence, the RBF kernel is further used to compare with ANN and NB classifiers. As for the ANN classifier, the most optimum epoch is at 1000 with a scaled conjugate gradient as the training algorithm. In addition, for the NB classifier, kernel distribution showed higher accuracy than the normal distribution. Hence kernel distribution is chosen for the NB classifier. From Table 6, the ANN classifier attains the highest accuracy at 94.22% for the DIR Set 1 gait feature that represents by the set of body points for the full body whilst the highest accuracy for the REF feature is at 89.98% based on Set 6, which is the set of distance for the entire body.

Similarly, the highest sensitivity and specificity are from the same sets, precisely 94.49% and 93.93% for Set 1 and 90.95% and 89.05% for Set 6. As for the SVM classifier, the highest accuracy achieved is at 92.17% for the DIR Set 2 gait feature that represented the body points for the upper body, whilst for the REF feature; Set 6 surpassed others with 91.67% accuracy along with sensitivity and specificity at 89.30% and 94.32% respectively. Conversely, the NB classifier showed the lowest accuracy compared to ANN and SVM classifiers. Set 1 and Set 6 only attained an accuracy of 78.83% and 72.50%, respectively, compared to other sets. On the other hand, set 1 achieved maximum sensitivity and specificity at 85.02% and 74.50%, respectively. However, set 6 only achieved maximum specificity at 69.56% and set 10 with a sensitivity of 76.59%. Overall, the ANN classifier outperformed the other two classifiers, specifically the SVM and NB, with NB as the lowest accuracy rate based on the computed performance measures.

TABLE 6. Performance measures (%) using ANN, SVM and NB as classifier

Classifier ANN				
Feature	Set	Acc	Sens	Spec
DIR	1	94.22	94.49	93.93
	2	91.78	92.88	90.73
	3	93.17	93.83	92.51
	4	91.90	92.81	91.02
	5	93.28	93.41	93.15
REF	6	89.98	90.95	89.05
	7	81.65	84.24	79.42
	8	84.72	84.68	84.75
	9	87.80	87.92	87.67
	10	83.15	84.90	81.56
Classifier SVM				
DIR	1	87.83	82.15	95.95
	2	92.17	91.21	93.17
	3	88.67	87.18	90.27
	4	90.17	88.49	91.98
	5	90.33	87.81	93.21
REF	6	91.67	89.30	94.32
	7	83.00	83.22	82.78
	8	85.83	86.19	85.47
	9	89.33	87.82	90.97
	10	84.67	85.37	83.98
Classifier NB				
DIR	1	78.83	85.02	74.50
	2	78.00	84.14	73.12
	3	77.17	83.82	72.70
	4	78.00	84.14	73.72
	5	77.33	84.17	72.77
REF	6	72.50	76.47	69.56
	7	71.33	77.11	67.58
	8	63.67	67.08	61.38
	9	68.83	72.87	66.00
	10	70.83	76.59	67.12

The ANN classifier attained the highest accuracy is at 94.22%, as achieved by the ANN classifier in this study, and outperformed other marker-based models that utilised ANN as classifiers (C.Z.C. Hasan et al. 2018 & S. Ilias et al. 2016). This finding suggests that the DIR Set 1 gait feature is suitable to be used as a potential gait feature to support the early diagnosis of ASD gait since the proposed method does not require any protocol experiments. The proposed markerless-based technique has fewer experimental protocols than the marker-based technique, which is more accommodating and more comfortable, especially for ASD children. Thus, the gait features can be extracted without contact with the subject. Recall that in this study, a single depth camera is used. Therefore, future studies could utilise multiple depth cameras at different locations to provide more multi-views to extract more significant gait features.

CONCLUSION

In conclusion, the gait classifications based on three classifiers, namely ANN, SVM and NB, are evaluated and validated in classifying two feature sets, namely DIR and FIR. Results showed that the ANN model classifies the

markerless-based gait feature between the ASD and TD group with the highest accuracy at 94.22% using DIR Set 1, representing the full-body based on extraction by selecting all body points in x, y, and z axes. Additionally, this feature set can classify the ASD group based on the sensitivity value achieved as 94.49% and the TD group with a specificity of 93.93%. However, the NB classifier is not apt for these feature sets. This quantitative proposed gait features and the classifier-based approach may help the medical practitioners to discriminate walking gait features into significant gait types that could assist them in performing an initial diagnosis related to gait abnormalities. Findings from this work are beneficial for future applications in facilitating appropriate therapeutic interventions for ASD children that need therapies and post-therapy monitoring in the field of pathological gait. This study used a single camera view to investigate the kinematic features based on the cosine rule. Hence for future work, multiple camera views could be analysed using kinematic features from the anatomical plane by comparing the relative orientations of the two segments and using the spatial-temporal and kinetic features based on the markerless-based gait technique.

ACKNOWLEDGEMENT

This research is funded by Research Management Centre (RMC), Universiti Teknologi MARA (UiTM), Shah Alam, Selangor, Malaysia Grant No: 600-IRMI/ MyRA5/3/ BESTARI (041/2017). The authors would like to thank UiTM for the facilities provided for this research namely the Human Motion and Gait Analysis Premier Laboratory and both guidance, volunteered participants and educators from the National Autism Society of Malaysia (NASOM).

DECLARATION OF COMPETING INTEREST

None

REFERENCES

B.O. Lim, D. O'Sullivan, B.-G. Choi, and M.-Y. Kim 2016. Comparative gait analysis between children with autism and age-matched controls: Analysis with temporal-spatial and foot pressure variables. *Journal of Physical Therapy Science* 28: 286-292. https://doi.org/10.1589/jpts.28.286

C. Armitano, H. Bennett, J. Haegele, and S. Morrison, 2020. Assessment of the gait-related acceleration patterns in adults with autism spectrum disorder. *Gait & Posture* 75: 155-162. http://dx.doi.org/10.1016/j.gaitpost.2019.09.002

C. C. Barreira, A. Forner-Cordero, P. M. Grangeiro, and R. T. Moura 2020. Kinect v2 based system for gait assessment of children with cerebral palsy in rehabilitation settings. *Journal of Medical Engineering & Technology,* 1-5. https://doi.org/10.1080/03091902.2020.1759709

C. Z. C. Hasan, R. Jailani, and N. M. Tahir 2018. ANN and SVM classifiers in identifying autism spectrum disorder gait based on three-dimensional ground reaction forces. *(Proceedings of TENCON 2018),* 2018 2436-2440. https://doi.org/10.1109/TENCON.2018.8650468

E. I. de Bruin, R. Blom, F. M. Smit, F. J. van Steensel, and S. M. Bögels. 2015. MYmind: Mindfulness training for youngsters with autism spectrum disorders and their parents. *Autism* 19: 906-914. https://doi.org/10.1177/1362361314553279

F. Sun, W. Zang, R. Gravina, G. Fortino, and Y. Li 2020. Gait-based identification for elderly users in wearable healthcare systems. *Information Fusion* 53: 134-144. https://doi.org/10.1016/j.inffus.2019.06.023

H. Bakhta, B.A. Nahla, Z. Elouedi, K. Mellouli 2009. Naïve possibilistic network classifiers, *Fuzzy Sets and Systems* 160(22): 3224-3238. https://doi.org/10.1016/j.fss.2009.01.009

H. L. Miller, P. M. Caçola, G. M. Sherrod, R. M. Patterson, and N. L. Bugnariu. 2019. Children with autism spectrum disorder, developmental coordination disorder, and typical development differ in characteristics of dynamic postural control: A preliminary study. *Gait & Posture* 67: 9-11. https://doi.org/10.1016/j.gaitpost.2018.08.038

I. Cocchi, G. Figari, N. Valeri, G. Paolini, U. Della Croce, A. Cereatti, E. Pantzar, A. Magnuson, and J. Riad. 2019. A 2D markerless gait analysis protocol to estimate the sagittal joint kinematics of children with cerebral palsy. *(Proceedings of 2019 IEEE 23rd International Symposium on Consumer Technologies (ISCT), 2019),* 192-196. https://doi.org/10.1109/ISCE.2019.8901029

J. D. Eggleston, J. R. Harry, and J. S. Dufek. 2018. Lower extremity joint stiffness during walking distinguishes children with and without autism. *Human Movement Science* 62: 25-33. https://doi.org/10.1016/j.humov.2018.09.003

J. D. Eggleston, J. R. Harry, P. A. Cereceres, A. N. Olivas, E. A. Chavez, J. B. Boyle, and J. S. Dufek. 2020. Lesser magnitudes of lower extremity variability during terminal swing characterizes walking patterns in children with autism. *Clinical Biomechanics* 76: 1-18. https://doi.org/10.1016/j.clinbiomech.2020.105031

J. S. Dufek, J. D. Eggleston, J. R. Harry, and R. A. Hickman. 2017. A comparative evaluation of gait between children with autism and typically developing matched controls. *Medical Sciences* 5(1): 1-11. https://doi.org/10.3390/medsci5010001

K. Jun, Y. Lee, S. Lee, D.-W. Lee, and M. S. Kim. 2020. Pathological gait classification using kinect v2 and gated recurrent neural networks. *IEEE Access* 8: 139881-139891. https://doi.org/10.1109/ACCESS.2020.3013029

K. Pope, J. Doll, A. Kyvelidou, H. Stessman, K. Nelson, and L. Jordan. 2020. Clinician, caregiver and patient perspectives of the continuum of care for autism. *Journal of Interprofessional Education & Practice* 19: 100335. https://doi.org/10.1016/j.xjep.2020.100335

L. Gong, Y. Liu, L. Yi, J. Fang, Y. Yang, and K. Wei. 2020. Abnormal gait patterns in autism spectrum disorder and their correlations with social impairments. *Autism Research* 13(7): 1215-1226. https://doi.org/10.1002/aur.2302

M. Calhoun, M. Longworth, and V. L. Chester. 2011. Gait patterns in children with autism. *Clinical Biomechanics* 26: 200-206. https://doi.org/10.1016/j.clinbiomech.2010.09.013

M. Galinium, J. Yapri, and J. Purnama. 2019. Markerless motion capture for 3D human model animation using depth camera. *TELKOMNIKA* 17(3): 1300-1309. http://dx.doi.org/10.12928/telkomnika.v17i3.8939

M. Leo, G. Medioni, M. Trivedi, T. Kanade, and G. Farinella. 2017. Computer vision for assistive technologies. *Computer Vision and Image Understanding* 154: 1-15. https://doi.org/10.1016/j.cviu.2016.09.001

M. Nieto-Hidalgo, F. J. Ferrández-Pastor, R. J. Valdivieso-Sarabia, J. Mora-Pascual, and J. M. García-Chamizo. 2015. Vision based extraction of dynamic gait features focused on feet movement using RGB camera. *Ambient Intelligence for Health,* 155-166. http://dx.doi.org/10.1007/978-3-319-26508-7_16

M. Nieto-Hidalgo, F. J. Ferrández-Pastor, R. J. Valdivieso-Sarabia, J. Mora-Pascual, and J. M. García-Chamizo. 2016. A vision-based proposal for classification of normal and abnormal gait using RGB camera. *Journal of biomedical informatics* 63: 82-89. https://doi.org/10.1016/j.jbi.2016.08.003

M. S. Nadeem, F. A. Al-Abbasi, I. Kazmi, B. N. Murtaza, M. A. Zamzami, M. A. Kamal, A. Arif, M. Afzal, and F. Anwar. 2020. Multiple risk factors: A challenge in the management of autism. *Current Pharmaceutical Design* 26: 743-754. https://doi.org/10.2174/1381612826666200226101218

N. M. Tahir, A. Hussain, M. M. Mustafa, S. A. Samad and H. Husin. 2007. Fourier Descriptor for Pedestrian Shape Recognition using Support Vector Machine. *(Proceedings of 2007 IEEE International Symposium on Signal Processing and Information Technology)*, 2007, 636-641. https://doi.org/10.1109/ISSPIT.2007.4458054

O. Manicolo, M. Brotzmann, P. Hagmann-von Arx, A. Grob, and P. Weber. 2019. Gait in children with infantile/atypical autism: Age-dependent decrease in gait variability and associations with motor skills. *European Journal of Paediatric Neurology* 23: 117-125. https://doi.org/10.1016/j.ejpn.2018.09.011

R. Sahak, N. M. Tahir, A. I. Yassin, F. K. Zaman, and A. Zabidi. 2017. Frontal view gait recognition using locally linear embedded and multilayer perceptron based on Kinect. (*Proceedings of Colloquium of Signal Processing & its Applications (CSPA) 2017),* 2017, 303-308. https://doi.org/10.1109/CSPA.2017.8064970

S. Ilias, N. M. Tahir, R. Jailani, and C. Z. C. Hasan. 2016. Classification of autism children gait patterns using Neural Network and Support Vector Machine. *(Proceedings of IEEE Symposium on Computer Applications & Industrial Electronics (ISCAIE) 2016)* 2016, 52-56. https://doi.org/10.1109/ISCAIE.2016.7575036

S. Ilias, N. M. Tahir, and R. Jailani. 2016. Feature extraction of autism gait data using principal component analysis and linear discriminant analysis. *(Proceedings of Industrial Electronics and Applications Conference (IEACon), 2016),* 2016, 275-279. https://doi.org/10.1109/IEACON.2016.8067391

S. J. Spence, P. Sharifi, and M. Wiznitzer. 2004. Autism spectrum disorder: screening, diagnosis, and medical evaluation. (*Seminars in Pediatric Neurology) 2004*, 186-195. https://doi.org/10.1016/j.spen.2004.07.002

Y. Li, R. M. Koldenhoven, T. Liu, and C. E. Venuti. 2021. Age-related gait development in children with autism spectrum disorder. *Gait & Posture* 84: 260-266. https://doi.org/10.1016/j.gaitpost.2020.12.022